

# ARN-LSTM: A Multi-Stream Attention-Based Model for Action Recognition with Temporal Dynamics

Chuanchuan WANG<sup>1</sup>, Ahmad Sufril Azlan Mohmamed<sup>1</sup>, Xiao Yang<sup>1</sup>, Xiang Li<sup>2</sup>

<sup>1</sup> School of Computer Science, Universiti Sains Malaysia, Penang, 11800, Malaysia

<sup>2</sup> School of Engineering, College of Technology and Business, Guangzhou, 510850, China

Corresponding author: Ahmad Sufril Azlan Mohamed ([sufril@usm.my](mailto:sufril@usm.my))

**Abstract:** This paper presents ARN-LSTM, a novel multi-stream action recognition model designed to address the challenge of simultaneously capturing spatial motion and temporal dynamics in action sequences. Traditional methods often focus solely on spatial or temporal features, limiting their ability to comprehend complex human activities fully. Our proposed model integrates joint, motion, and temporal information through a multi-stream fusion architecture. Specifically, it comprises a joint stream for extracting skeleton features, a temporal stream for capturing dynamic temporal features, and an ARN-LSTM block that utilizes Time-Distributed Long Short-Term Memory (TD-LSTM) layers followed by an Attention Relation Network (ARN) to model temporal relations. The outputs from these streams are fused in a fully connected layer to provide the final action prediction. Evaluations on the NTU RGB+D 60 and NTU RGB+D 120 datasets demonstrate the effectiveness of our model, achieving effective performance, particularly in group activity recognition.

**Keywords:** Multi-Stream, Long Short-Term Memory, Attention Relation Network, Action Recognition

## 1. Introduction

Action recognition is a key task in computer vision, with applications spanning human-computer interaction, video surveillance, healthcare, and robotics<sup>[1, 2]</sup>. Recent advancements have significantly improved the accuracy of action recognition models, yet challenges remain, particularly in effectively capturing both spatial and temporal dynamics in human activity sequences. Human action recognition methods can be classified into two primary categories: RGB-based and skeleton-based<sup>[3, 4]</sup>. The latter extracts skeleton points from input videos, modeling their feature changes across frames to facilitate action recognition. Compared to RGB-based methods<sup>[5-7]</sup>, these approaches lower hardware demands and computational costs, while being less vulnerable to interference from extraneous factors such as lighting or background<sup>[8]</sup>. Traditional methods either focus on spatial or temporal information in isolation, limiting their ability to understand complex activities involving motion and temporal patterns fully. Traditional skeleton-based interaction recognition approaches treat human joints as independent features, constructing feature sequences from them for input into recurrent or convolutional neural networks to predict actions. However, these methods fail to account for the correlation features between different joints<sup>[9]</sup>.

Most existing single-person<sup>[8, 10]</sup> action recognition methods have adopted the concept of graph convolution. However, in action recognition, scenarios often involve both dual-person interactions and single-person movements. Traditional graph convolution models typically treat the two individuals in dual-person interactions as isolated entities, thereby neglecting critical interaction information between them.

Therefore, to effectively extract the interaction information between behaviors and be inspired by

the the effectiveness of feature fusion idea<sup>[11-14]</sup>, we propose the ARN-LSTM architecture for human action recognition. The ARN-LSTM approach is a multi-stream action recognition model designed to fuse joint, motion, and temporal features to address these challenges. Our model leverages Attention Relation Networks (ARN)<sup>[15]</sup> to enhance the correlations between these features, allowing for more comprehensive action recognition. By combining joint skeletal data with temporal dynamics, ARN-LSTM provides a more complete understanding of human activity, this fusion of streams allows ARN-LSTM to handle more complex action sequences, particularly in group activity recognition tasks.

The key contributions of this work are summarized as follows:

1. We proposed a multi-stream architecture that fuses joint, motion, and temporal information for improved action recognition, significantly enhancing action recognition capabilities. It serves to perform fusion among multiple relational models and accommodates various fusion types (e.g., separate individual models, interrelational models, etc.). This approach flexibly integrates diverse forms of relational information to construct the final input feature representation.
2. This work introduces the Attention Relation Network (ARN), a novel mechanism designed to effectively capture and amplify the interrelationships between spatial and temporal features, thereby refining the model's analytical prowess.
3. Our model achieves effective performance on the NTU RGB+D 60/120 dataset, demonstrating its robust capacity to manage and interpret complex group activities with high precision.

These contributions culminate in the innovative architecture ARN-LSTM, which is both straightforward and effective. We conduct experiments on the largest and most widely used action-recognition dataset encompassing human interactions across varied conditions, achieving state-of-the-art performance and competitive results that underscore the robustness of our proposed approach.

This paper is organized as follows: Section 2 discusses related work in action recognition. Section 3 Explains our proposed ARN-LSTM model, including its multi-stream architecture, the TD-LSTM architecture and fusion mechanism. Section 4 outlines the experimental setup, including the dataset, evaluation metrics, and implementation details. Section 5 presents the results and discusses the model's performance, followed by a conclusion in Section 6.

## **2. Related Work**

Action recognition has seen considerable advancements with the rise of deep learning techniques, particularly convolutional neural networks (CNNs) and recurrent neural networks (RNNs)<sup>[16]</sup>. Traditional methods can be broadly classified into two categories: spatial-based, temporal-based, and spatial-temporal-based approaches. This section will briefly review the related works about the three fields of skeleton-based action recognition.

### **2.1 Spatial-based Approaches**

Spatial-based methods capture spatial features such as human poses, body parts, and skeletal structures. Early works primarily relied on hand-crafted features, which were limited in capturing complex motion patterns. With the advent of deep learning, CNN-based<sup>[17]</sup> approaches have emerged, significantly improving the ability to extract spatial features from video frames. Skeleton-based approaches, such as those that extract joint positions, have also gained popularity due to their robustness against variations in appearance and lighting.

### **2.2 Temporal-based Approaches**

Temporal-based methods, on the other hand, focus on modeling the temporal evolution of actions over time. Long Short-Term Memory (LSTM) networks and Temporal Convolutional Networks (TCNs) have widely captured temporal dependencies in action sequences. These models have demonstrated success

in handling the sequential nature of action data, yet they often struggle with long-range temporal dependencies and complex temporal dynamics. Early deep learning approaches in human activity recognition (HAR) typically employed CNN<sup>[18]</sup><sup>[5]</sup> or RNN<sup>[19]</sup><sup>[20]</sup> for temporal modeling. For example, Du et al.<sup>[18]</sup> applied 3D convolution to sequence segments to model temporal dynamics, pooling along the temporal dimension for the final feature representation. Another common approach involves converting sequences into 2D representations, with 2D CNNs<sup>[21]</sup><sup>[22]</sup> used to capture temporal dynamics. In studies such as<sup>[23]</sup> discrete joint trajectories were color-encoded to create 2D images, referred to as Joint Trajectory Maps, which were then processed using CNN-based models to extract temporal features. However, representing skeleton sequences as pseudo-images fails to fully capture the complex interconnectivity among human joints.

Recent models<sup>[24]</sup><sup>[25]</sup> employ temporal convolutions at three fixed scales<sup>[24]</sup> to capture long, medium, and short-term temporal graph convolution network characteristics of individual joints. This was further enhanced by incorporating spatially neighboring joints<sup>[26]</sup><sup>[27]</sup> when applying temporal convolutions. Zhifu et al.<sup>[28]</sup> extended this approach by incorporating predefined body parts, though such predefined parts may inevitably include non-informative joints. In<sup>[29]</sup>, sample-dependent weights were introduced during scale fusion. Notably, all of these multi-scale temporal methods rely on conventional average or max pooling for feature aggregation<sup>[24]</sup><sup>[29]</sup>.

### 2.3 Multi-stream Fusion Models

Multi-stream architectures that integrate both spatial and temporal features have shown promise in overcoming the limitations of single-stream models<sup>[30]</sup><sup>[31]</sup>. Two-stream networks<sup>[8]</sup>, for example, process spatial and temporal information in parallel using separate CNNs for RGB frames and optical flow, and later fuse the outputs<sup>[32]</sup>. Although these models provide improved accuracy, they still suffer from limited fusion mechanisms that do not fully capture the interdependencies between spatial and temporal features, such as the motion interaction relation information.

Overall, existing methods face limitations in the simultaneous selection of discriminative frames and joints during temporal pooling. Furthermore, they struggle to model the long-range cross-joint relationships among informative joints effectively. The proposed ARN-LSTM aims to address these challenges. Our ARN-LSTM model builds on this idea of multi-stream fusion but introduces a more sophisticated fusion mechanism using Attention Relation Networks, enabling a deeper integration of spatial and temporal features.

## 3. Proposed ARN-LSTM Model

In this section, we describe the architecture of the ARN-LSTM model and its key components. Previous research indicates that the simultaneous use of different streams can significantly improve the performance of human action recognition<sup>[33]</sup>. Consequently, we assess the performance of the trained models employing streams for joint, bone, joint motion, and bone motion. The bone stream uses bone modality as input data, as proposed by Shi et al.<sup>[34]</sup> The joint motion and bone motion streams are consistent with the methodology outlined by Shi et al.<sup>[33]</sup>. The final result is determined by calculating a weighted average of the inference outputs from the models.

### 3.1 Model Overview

Inspired by the RN<sup>[35]</sup>, IRN<sup>[36]</sup> and ARN<sup>[15]</sup> architecture, we designed an ARN-LSTM method. The architecture drove three interaction relationships: inward-person relationships, outward-person relationships, and the two features fusing relations.

Define a sophisticated neural network architecture designed to process inputs involving diverse objects (e.g., human body joint data) while employing relational modeling and attention mechanisms to

enhance model performance. This architecture is particularly suited for handling complex data characterized by multiple inputs and relationships, especially in tasks such as behavior recognition or human posture estimation. With its flexible parameter configurations, users can adapt the model structure to fulfill specific task requirements.

In the selection of weights during the relational modeling process, a Gaussian<sup>[37, 38]</sup> function was employed to generate weights that prioritize the central sequence. The Gauss formula is shown in (1):

$$gauss(x) = \frac{1}{\sigma\sqrt{2\pi}} \exp\left(-\frac{x^2}{2\sigma^2}\right) \quad (1)$$

For the inward-person relation use as  $ARN - LSTM_{inward}(P_1, P_2)$  corresponding to equations (2):  
 $ARN - LSTM_{inward}(P_1, P_2) =$

$$f_{\phi}\left(\sum_{i,k} g_{\theta}(j_i^1, j_k^2) \oplus \sum_{i,k} g_{\theta}(j_i^2, j_k^1)\right) \quad (2)$$

In theory,  $f_{\phi}$  and  $g_{\theta}$  can represent Multi-Layer Perceptrons (MLPs) characterized by trainable parameters  $\phi$  and  $\theta$ , respectively<sup>[15]</sup>. Notably, it  $\oplus$  can encompass various pooling operations, including summation, maximization, averaging, or concatenation<sup>[36]</sup>. However, based on our experimental findings, we have opted to employ the averaging operation due to its superior performance.

For the outward-person relation is  $ARN - LSTM_{outward}(P_1, P_2)$  corresponding to equations (3):

$$ARN - LSTM_{outward}(P_1, P_2) = f_{\phi'}\left(\sum_{i=1}^N \sum_{K=i+1}^N g_{\theta}(j_i^1, j_K^1)\right) \quad (3)$$

Recognizing that intra-personal relationships among joints can provide critical insights, we propose an innovative architecture wherein the joints of each individual are paired exclusively with their corresponding joints. In this framework, bidirectional pairing is superfluous since the joint pairs stem from a single individual. Our preliminary experiments indicate that incorporating bidirectional pairing may introduce redundant complexity into the model, potentially leading to overfitting in certain cases. This finding underscores the necessity for a more streamlined approach to joint pairing that retains essential structural relationships while minimizing extraneous redundancy. By focusing on the inherent relationships within an individual's joint configuration, our architecture aims to enhance model efficiency and generalization. This streamlined design not only simplifies the computational requirements but also fortifies the robustness of the recognition process. Our observations suggest that eliminating unnecessary bidirectional connections could pave the way for improved accuracy and interpretability in human action recognition tasks. Thus, we advocate for a paradigm shift towards leveraging intra-personal joint relationships as a foundational element in the design of action recognition architectures, with the potential to yield significant advancements in the field. The aggregated output from each individual is concatenated ( $\cap$ ) before being processed through function  $f$ , characterized by its trainable parameters  $\phi$ .

$ARN - LSTM_{inward+outward}(P_1, P_2)$  represents for the inward-person and outward-person fusion relation, corresponding to equations (4):

$$\begin{aligned}
ARN - LSTM_{inward+outward}(P_1, P_2) = f_{\emptyset''} & \left( \sum_{i,k} g_{\theta}(j_i^1, j_k^2) \oplus \sum_{i,k} g_{\theta}(j_i^2, j_k^1) \sum_{i=1}^N \sum_{k=i+1}^N g_{\Theta}(j_i^1, j_k^1) \right. \\
& \left. \cap \sum_{i=1}^N \sum_{k=i+1}^N g_{\Theta}(j_i^2, j_k^2) \right) \quad (4)
\end{aligned}$$

The relationship modeling module constructs distinct relationship matrices according to the specified type of relationship (e.g., intra-monadic relationships, inter-individual relationships) and processes each pair of input objects through the  $g_{\theta}$  network. Conclusively, we propose an architecture that amalgamates both categories of relationships within a unified function  $f$  (parametrically defined by  $\emptyset$ ), achieved through concatenating the pooled information from each function  $g$ , each governed by its distinct parameters  $\theta$  and  $\Theta$ .

The ARN-LSTM model is designed to capture both spatial and temporal features in action recognition tasks. The model comprises three primary components: the joint stream, the temporal Stream, and the ARN-LSTM block(the ARN method with LSTM layers). Each stream processes distinct aspects of the input data, which are then fused to generate the final action prediction<sup>[15]</sup>.

(1) The joint stream

The Joint stream focuses on extracting spatial features from the human skeleton. By leveraging skeletal data, the model captures spatial configurations of human joints, critical for identifying poses and movements.

(2) The temporal stream

The Temporal stream captures temporal dynamics in the input sequence. This stream models the evolution of joint movements over time, providing insights into the dynamic nature of actions.

(3) The Time distributed Long short-term memory block

The ARN-LSTM block is the model's core and captures both short- and long-term temporal dependencies. It consists of Temporal-Deep Long Short-Term Memory (TD-LSTM) layers and an Attention Relation Network (ARN)<sup>[15]</sup>. The TD-LSTM layers model temporal relationships within each stream, while the ARN enhances the correlations between the joint and temporal features, allowing the model to focus on the most relevant aspects of the action sequence.

### 3.3 TD-LSTM block

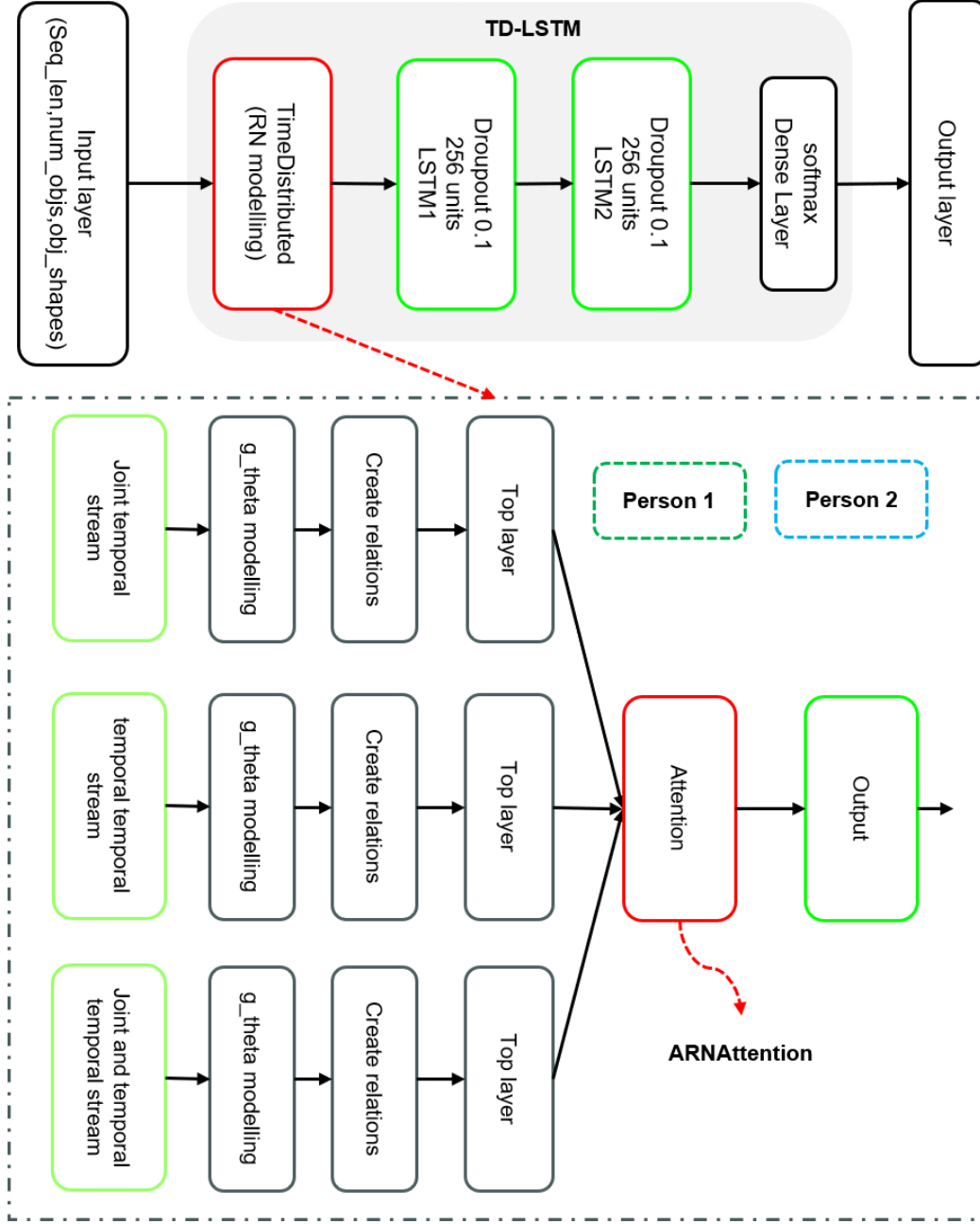


**Figure 1 Illustration of the proposed Time Distributed LSTM architecture**

The Time Distributed LSTM (TD-LSTM) comprises the main components depicted in Figure 1. The input layer consists of several objects, each with a specific object shape dimension. The distributed layer applies the same neural network across the time dimension, while the LSTM component includes two separate LSTM layers for time series processing. The dense layer, serving as the output layer, utilizes the softmax activation function to generate the final output. Note that in Timedistributed layer, the person-to-person relationship model needs to be taken into account, and the input sequences include joint stream with motion, temporal stream with motion, and joint fused temporal with motion, separately. For a detailed insight into the TD-LSTM method flow, please refer to Algorithm 1.

---

**Algorithm 1** The LSTM Integration with Temporal Distributed Model

---

---

**Input:**

- object\_shape: Shape of each object
- seq\_len: Sequence length
- prune\_at\_layer: Pruning layer
- kernel\_init: Kernel initializer
- g\_theta\_kwargs:
- drop\_rate: Dropout rate

**Output:** The Compiled Temporal Relation Network model

```
1: g_theta_model ← initialize_g_theta(object_shape, kernel_init, **g_theta_kwargs)

2: if prune_at_layer is not None:

3:     for layer in reversed(g_theta_model.layers):

4:         if layer_name ends with prune_at_layer:

5:             top_layer_out ← layer.output

6:             break

7:     g_theta_model ← Model(inputs=g_theta_model.input, outputs=top_layer_out)

8: input_g_theta ← create_input(shape=((2,)+object_shape))

9: g_theta_model_out ← g_theta_model(Lambda(slice_input)(input_g_theta))

10: merged_g_theta_model ← Model(inputs=input_g_theta, outputs=g_theta_model_out)

11: temporal_input ← create_input(shape=((seq_len, 2,) + object_shape))

12: x ← TimeDistributed(merged_g_theta_model)(temporal_input)

13: x ← LSTM(500, dropout=drop_rate, return_sequences=True)(x)

14: g_theta_lstm_model ← Model(inputs=temporal_input, outputs=x, name='g_theta_lstm')

15: return g_theta_lstm_model
```

---

### 3.2 Multi-stream Fusion

After processing the input data through the three streams, the outputs are fused using a fully connected layer. This fusion layer combines the spatial and temporal features, enabling the model to represent the action comprehensively. The fused features are then passed through a final softmax layer to produce the action prediction. The overview of the proposed ARN-LSTM method is shown in Figure 2.

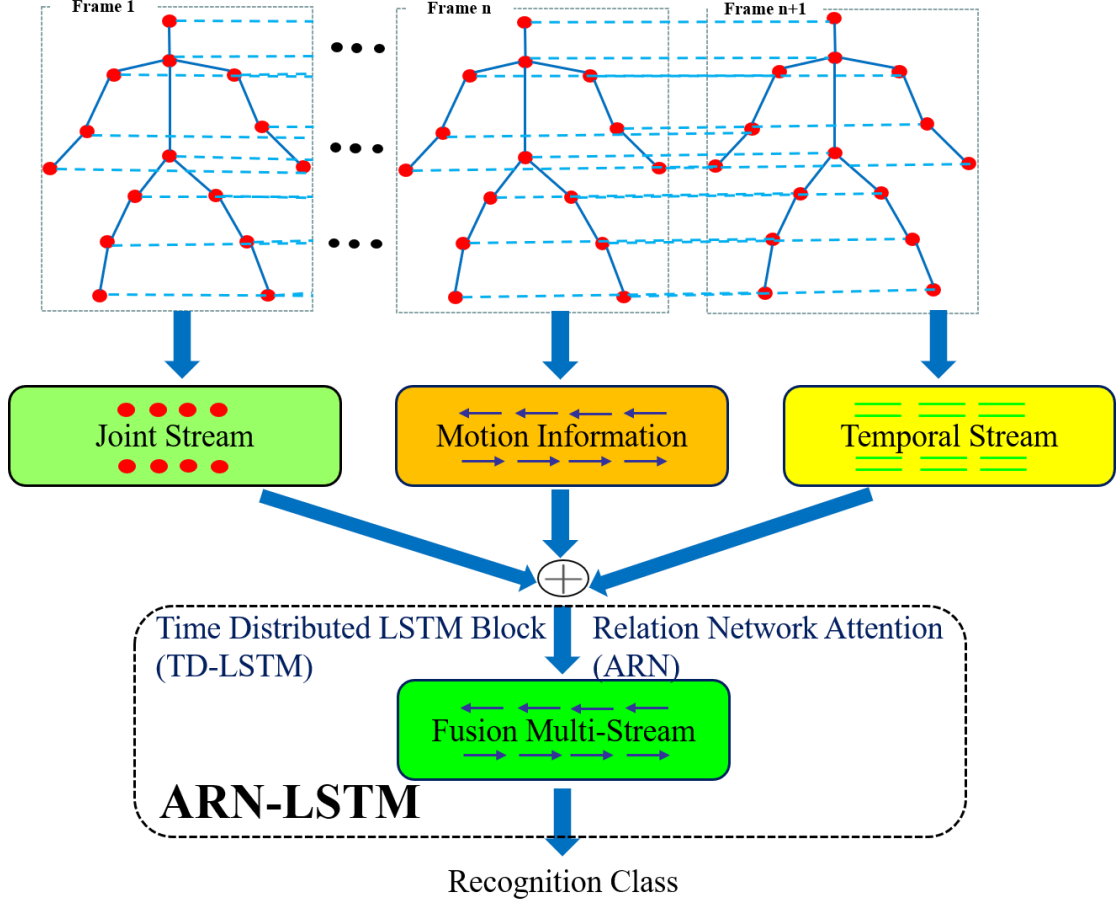


**Figure 2** The overview of the proposed ARN-LSTM method

This approach constructs a sophisticated neural network model adept at processing diverse forms of object data, including federated streams, joint streams, temporal streams, and general relational data. It leverages relational modeling and attention mechanisms to enhance model performance. The flexible parameter configuration facilitates the implementation of various network architectures.

## 4. Experimental Setup

### 4.1 Dataset

The ARN-LSTM model was evaluated on the NTU RGB+D 60 and NTU RGB+D 120 datasets. The NTU RGB+D dataset is the largest and most widely used action-recognition dataset.

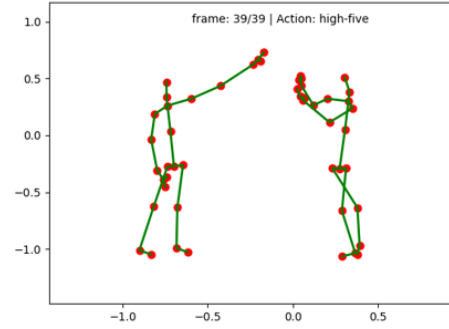
**NTU RGB+D dataset.** The NTU RGB+D 60<sup>[39]</sup> dataset comprises 56,880 skeleton action sequences across 60 classes. Each sample represents a single action, performed by up to two subjects and recorded by three cameras from varying perspectives. The dataset is partitioned into two test benchmarks based on distinct subjects and views: cross-subject (or X-Sub) and cross-view (or X-View).

**NTU RGB+D 120 dataset.** The NTU RGB+D 120 dataset extends the NTU RGB+D collection, comprising 114,480 samples across 120 classes<sup>[40]</sup>. This dataset was captured using three cameras and encompasses 32 settings, each representing a specific location and background. It is organized into two

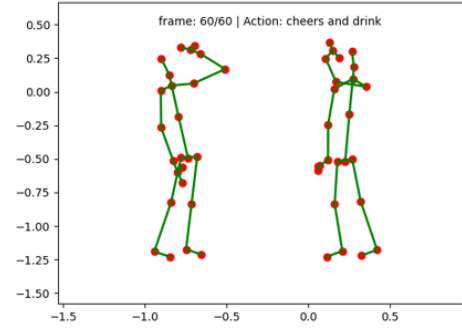


benchmarks based on subject parity and sample IDs: cross-subject (or X-Sub) and cross-setup (or X-View). The dataset includes both RGB frames and 3D skeleton data, making it ideal for evaluating the performance of multi-stream models like ARN-LSTM.

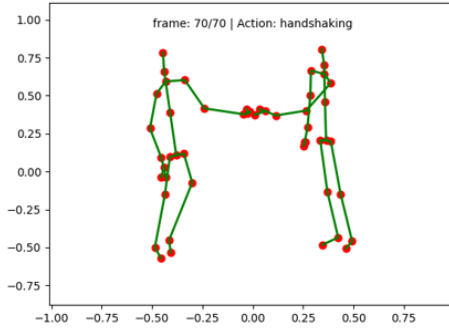
The skeletons should generate a single CSV file with all the normalized coordinates in this work. The datasets used or analyzed during the current study are publicly available from the link <https://doi.org/10.6084/m9.figshare.27427188.v1>. 26 mutual actions were used for evaluation, and Openpose extracted four sample skeleton-based interaction actions, shown in Figure 3.



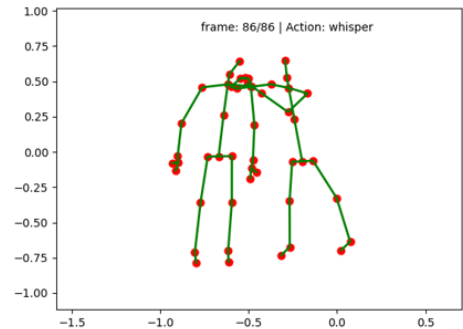
(a) High-five



(b) Cheers and drink



(b) Handshaking



(d) Whisper

**Figure 3 Sample skeleton actions of the NTU RGB+D dataset.(a) high-five,(b)cheers and drink,(c)handshaking and(d)whisper.**

## 4.2 Evaluation Metrics

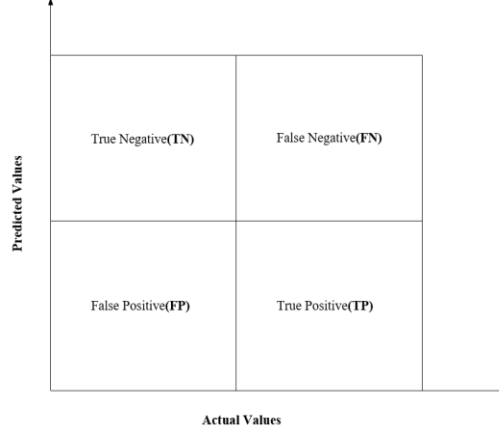


**Figure 4 Example of confusion matrix.**

We used standard metrics for action recognition evaluation, including accuracy, precision, recall, and F1-score<sup>[41]</sup>. The confusion matrix was also analyzed to assess the model's robustness in differentiating between similar action classes. For the binary classification recognition problem, a confusion matrix is used to evaluate performance on test data shown in Figure 4, the Accuracy, Precision, Recall and F-Score equation as described in (5),(6),(7),(8) separately.

$$Accuracy = \frac{TP+TN}{TP+TN+FP+FN} \quad (5)$$

$$Precision = \frac{TP}{TP+FP} \quad (6)$$

$$Recall = \frac{TP}{TP+FN} \quad (7)$$

$$F - Score = 2 * \frac{Precision*Recall}{Precision+Recall} \quad (8)$$

In this matrix, True Positives (TP) represent correctly predicted positive samples, False Positives (FP) indicate incorrect predictions of positive samples, True Negatives (TN) represent correctly predicted negative samples, and False Negatives (FN) indicate incorrect predictions of negative samples. Key metrics such as accuracy, precision, recall, and F-score were employed to assess the performance of the proposed ARN-LSTM image classification framework.

#### 4.3 Implementation Details

The ARN-LSTM model was implemented using Tensorflow 2.8.0 and Python 3.8.16. The Joint and Temporal streams were initialized without pre-trained weights, and the ARN-LSTM block was trained from scratch. The model was optimized using Adam with a learning rate of 0.0001. The training was conducted on a single NVIDIA RTX4090 GPU, with a batch size of 64, a learning rate of 0.0001, a drop rate of 0.1 and early stopping based on validation accuracy.

#### 4.4 Comparison of multi-stream feature

We experiment with the proposed approach of multi-stream feature comparisons, acknowledging that coordinates are not wholly accurate and often contain noise along with occasional tracking errors. To more precisely reflect the algorithm's performance, we employ a 5-fold cross-validation protocol to report each fold's accuracy of the ARN-LSTM approach.

Table 1 presents a performance comparison of ARN-LSTM models with different multi-stream fusion features (joint, temporal, and motion) on the NTU RGB+D 60 dataset, evaluated on both cross-

subject and cross-view tasks.

**Table 1** Comparison of ARN-LSTM with multi-stream feature (containing joint, temporal and motion) methods on the NTU RGB+D 60 dataset

| Methods               | Fold no. | Cross-subject |             | Cross-view   |             |
|-----------------------|----------|---------------|-------------|--------------|-------------|
|                       |          | Acc(%)        | Loss        | Acc(%)       | Loss        |
| joint+motion          | 0        | 92.46         | 0.20        | 95.30        | 0.13        |
|                       | 1        | 95.74         | 0.13        | 91.57        | 0.24        |
|                       | 2        | 94.85         | 0.15        | 93.05        | 0.19        |
|                       | 3        | 95.66         | 0.13        | 93.57        | 0.18        |
|                       | 4        | 92.99         | 0.20        | 95.41        | 0.12        |
| temporal+motion       | 0        | 91.80         | 0.22        | 94.57        | 0.15        |
|                       | 1        | 95.22         | 0.13        | 92.89        | 0.19        |
|                       | 2        | 92.95         | 0.19        | 92.92        | 0.19        |
|                       | 3        | 93.82         | 0.16        | 93.64        | 0.18        |
|                       | 4        | 93.44         | 0.17        | 94.93        | 0.14        |
| Joint+temporal+motion | 0        | 91.16         | 0.24        | <b>98.62</b> | <b>0.05</b> |
|                       | 1        | <b>98.80</b>  | <b>0.03</b> | 98.58        | 0.04        |
|                       | 2        | 97.99         | 0.06        | 97.60        | 0.07        |
|                       | 3        | 98.50         | 0.04        | 96.11        | 0.11        |
|                       | 4        | 95.86         | 0.11        | 98.03        | 0.06        |

Three configurations are compared:

**Joint with motion:** For cross-subject, accuracy ranges from 92.46% to 95.74% with a loss between 0.13 and 0.20. For cross-view, accuracy ranges from 91.57% to 95.41% with a loss between 0.12 and 0.24.

**Temporal with Motion:** For cross-subject, accuracy ranges from 91.80% to 95.22% with a loss between 0.13 and 0.22. For cross-view, accuracy ranges from 92.89% to 94.93% with a loss between 0.14 and 0.19.

**Joint fusion temporal with motion:** For cross-subject, accuracy ranges from 91.16% to 98.80% with a loss between 0.03 and 0.24. For cross-view, accuracy ranges from 96.11% to 98.62% with a loss between 0.04 and 0.11.

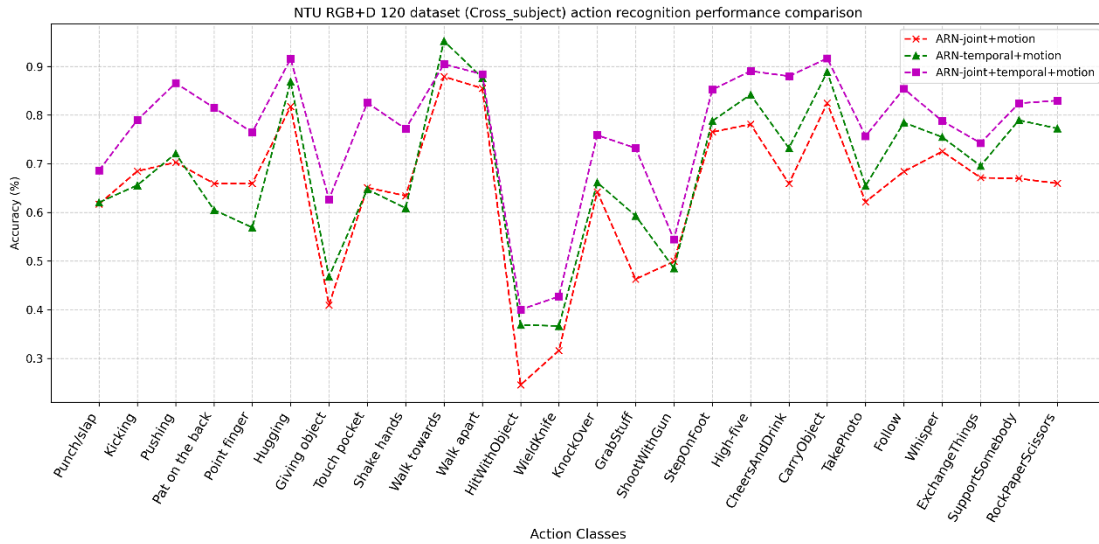
The Joint fusion temporal with motion configuration achieves the best performance, especially in cross-view tasks, where accuracy reaches 98.62%.

**Table 2** Comparison of ARN-LSTM with multi-stream feature (containing joint, temporal and motion information) methods on the NTU RGB+D 120 dataset

| Methods         | Fold no. | Cross-subject(%) |      | Cross-view(%) |      |
|-----------------|----------|------------------|------|---------------|------|
|                 |          | Acc(%)           | Loss | Acc(%)        | Loss |
| joint+motion    | 0        | 92.01            | 0.23 | 91.97         | 0.23 |
|                 | 1        | 93.04            | 0.20 | 91.66         | 0.24 |
|                 | 2        | 86.12            | 0.10 | 93.34         | 0.20 |
|                 | 3        | 93.92            | 0.17 | 91.89         | 0.24 |
|                 | 4        | 91.44            | 0.25 | 93.90         | 0.18 |
| temporal+motion | 0        | 91.39            | 0.24 | 92.14         | 0.22 |
|                 | 1        | 91.36            | 0.24 | 92.10         | 0.22 |

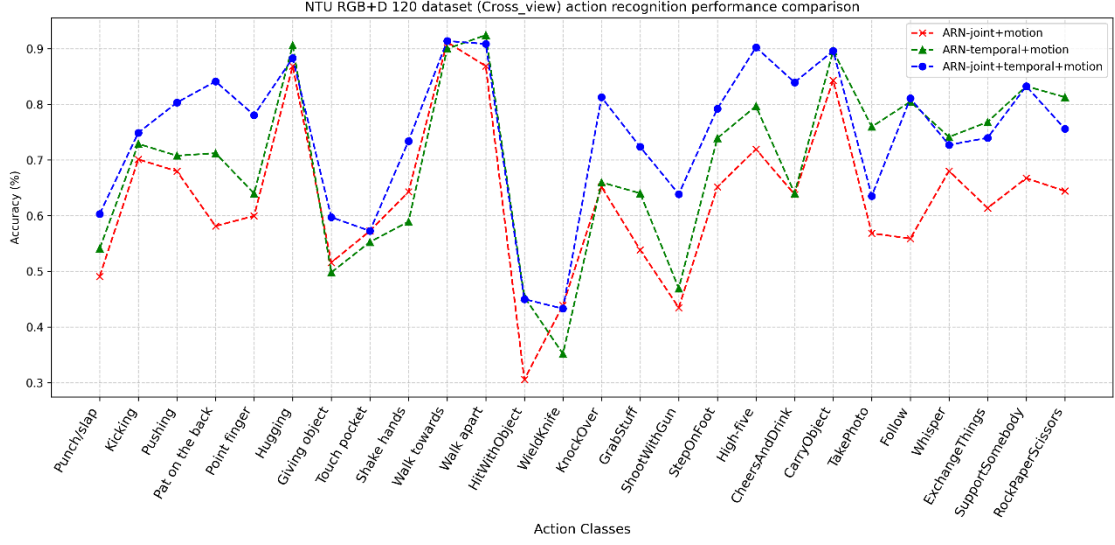
|                       |   |              |             |              |             |
|-----------------------|---|--------------|-------------|--------------|-------------|
|                       | 2 | 92.46        | 0.21        | 89.62        | 0.29        |
|                       | 3 | 90.07        | 0.28        | 91.72        | 0.23        |
|                       | 4 | 92.56        | 0.20        | 91.48        | 0.23        |
|                       | 0 | 98.74        | 0.04        | 96.70        | 0.10        |
|                       | 1 | 97.95        | 0.06        | 99.31        | 0.02        |
| Joint+temporal+motion | 2 | <b>99.47</b> | <b>0.02</b> | 99.22        | 0.03        |
|                       | 3 | 98.90        | 0.04        | <b>99.49</b> | <b>0.02</b> |
|                       | 4 | 97.87        | 0.07        | 99.09        | 0.03        |

Figure 5 presents action recognition accuracy comparisons for the NTU RGB+D 120 dataset (cross-subject) across various action classes using three fusion models: ARN-joint+motion, ARN-temporal+motion, and ARN-joint+temporal+motion. The ARN-joint+temporal+motion model (purple) consistently achieves higher accuracy across most action classes, notably outperforming the other models in actions such as “Hugging,” “Shake hands,” and “Wield knife.” In general, the ARN-temporal+motion model (green) performs better than the ARN-joint+motion model (red) in several action classes, though the performance gap varies across different actions.



**Figure 5 Different stream feature method's accuracy comparison in the NTU RGB+D 120 dataset with the Cross-subject benchmark.**

Figure 6 presents the comparison of action recognition accuracy across different classes using the NTU RGB+D 120 dataset (cross-view) for three fusion models: ARN-joint+motion, ARN-temporal+motion, and ARN-joint+temporal+motion. The ARN-joint+temporal+motion model (blue) consistently outperforms the other two, especially in actions like “Hugging,” “Shake hands,” and “Hit with object.” Performance varies significantly across action types, with some classes showing close performance between the models.



**Figure 6 Different stream feature method's accuracy comparison in the NTU RGB+D 120 dataset with the Cross-view benchmark.**

In summary, the two graphs compare action recognition performance on the NTU RGB+D 120 dataset (cross-view and cross-subject) across three fusion models, with ARN-joint+temporal+motion consistently outperforming ARN-joint+motion and ARN-temporal+motion across most action classes.

## 5. Results and Discussion

### 5.1 Performance Comparison

Experiment performance compared with the previous technical, to more precisely reflect the algorithm's superior performance, we leverage a 5-fold cross-validation protocol to report the top-1 accuracy of our approach.

Table 3 summarizes the performance of ARN-LSTM compared to other state-of-the-art methods on the NTU RGB+D 60 and 120 datasets. Our model achieved effective results, the accuracy has improved overall and outperforming traditional two-stream networks and temporal-only models. The incorporation of ARN significantly improved the model's ability to differentiate between similar actions, as evidenced by the confusion matrix in Figure 9, Figure 10 and Figure 11.

**Table 3** Compare with the previous method on the NTU RGB + D 60/120 dataset.

| Methods                      | Year | NTU RGB+D 60   |               | NTU RGB+D 120  |               |
|------------------------------|------|----------------|---------------|----------------|---------------|
|                              |      | Cross-setup(%) | Cross-view(%) | Cross-setup(%) | Cross-view(%) |
| ST-LSTM <sup>[42]</sup>      | 2016 | 69.2           | 77.7          | 55.7           | 57.9          |
| STA-LSTM <sup>[43]</sup>     | 2017 | 73.4           | 81.2          | --             | --            |
| ST-GCN <sup>[8]</sup>        | 2018 | 59.1           | 64.0          | 70.7           | 73.2          |
| 2s-AGCN <sup>[34]</sup>      | 2019 | 88.5           | 95.1          | 82.5           | 84.2          |
| 4s-shift-GCN <sup>[44]</sup> | 2020 | 90.7           | 96.5          | 85.9           | 87.6          |
| MCC+2s-AGCN <sup>[45]</sup>  | 2021 | 89.7           | 96.3          | 81.3           | 83.3          |
| EfficientGCN <sup>[46]</sup> | 2022 | 92.1           | 96.1          | 88.7           | 88.9          |
| PA-GCN <sup>[47]</sup>       | 2023 | 92.1           | 96.7          | 87.4           | 89.8          |
| ARN <sup>∗[15]</sup>         | 2023 | 93.0           | 93.6          | 92.1           | 93.3          |
| ARN-LSTM_inward              | --   | 97.1           | 97.2          | 94.9           | 91.8          |

|                         |    |             |             |             |             |
|-------------------------|----|-------------|-------------|-------------|-------------|
| ARN-LSTM_outward        | -- | 94.5        | 98.4        | 97.7        | 94.3        |
| ARN-LSTM_inward+outward | -- | <b>97.1</b> | <b>99.4</b> | <b>99.7</b> | <b>95.8</b> |

\*represents the results obtained from the reproduction of the paper.

Table 3 compares the performance of various action recognition models on the NTU-RGB+D 60 and NTU-RGB+D 120 datasets. The performance of these models is measured by two key accuracy metrics: Cross-Setup and Cross-View. In the context of action recognition, the Cross-Setup metric refers to a training and testing split where actions are captured from different spatial setups (camera locations), while Cross-View focuses on the generalization ability of models across different camera angles.

The ARN-LSTM models, evaluated specifically for inward, outward, and inward+outward variants, showcase a substantial leap in accuracy compared to previous methods. The inward ARN-LSTM variant achieves 97.1% for Cross-Setup and 97.2% for Cross-View, indicating excellent generalization across setups and views. The outward variant performs slightly lower in Cross-Setup with 94.5% but surpasses the inward variant in Cross-View with an impressive 98.4%. The combined inward+outward ARN-LSTM model achieves the highest accuracy scores of all methods listed, with 99.1% for Cross-Setup and 99.4% for Cross-View. These results highlight the ARN-LSTM architecture's ability to robustly capture both inward and outward skeletal motion dynamics, leading to near-perfect recognition performance on the NTU-RGB+D 60 dataset.

The ARN-LSTM models also show strong performance on the NTU-RGB+D 120 dataset, with the inward variant scoring 94.9% for Cross-Setup and 91.8% for Cross-View. The outward variant achieves slightly lower accuracies, with 97.7% in Cross-Setup and 94.3% in Cross-View. Finally, the inward+outward variant again outperforms the other methods, achieving a remarkable 99.7% for Cross-Setup and 95.8% for Cross-View. These results indicate that the ARN-LSTM models, especially the combined inward+outward variant, can scale to larger and more diverse datasets without compromising performance.

The ARN-LSTM models, particularly the inward+outward variant, set a new benchmark for performance on both the NTU-RGB+D 60 and NTU-RGB+D 120 datasets, achieving near-perfect accuracy scores. Models such as 4s-shift-GCN, EfficientGCN, and PA-GCN also demonstrate highly competitive performance, though the ARN-LSTM variants slightly outperform them. This progression underscores the importance of architectural innovations, particularly the incorporation of multi-stream, adaptive, and spatio-temporal modeling techniques, in advancing the field of action recognition.

## 5.2 Ablation Study

We conducted an ablation study to better understand each component's contribution by removing different parts of the ARN-LSTM architecture. The results, shown in Table 2, demonstrate that both the multi-stream fusion and ARN components are critical to the model's performance. Removing the ARN block, for example, resulted in a 5% decrease in accuracy, highlighting the importance of attention mechanisms in action recognition.

Table 4 presents our proposed ARN-LSTM approach, a comparative analysis of different fusion feature models for action recognition performance on the NTU-RGB+D 120 dataset using the Cross-View benchmark. The performance metrics are reported for three streams: joint-motion, temporal-motion, and joint-temporal-motion, with accuracy (Acc%), accuracy improvement (Acc( $\uparrow$ %)), and the most common misclassified actions (Similar Action) for each recognized action. Key observations include the superior performance of the joint-temporal-motion fusion model, which consistently improves

recognition accuracy for most actions, such as WalkTowards (91.4%) and ShakeHands (83.9%). Additionally, the Acc( $\uparrow$ %) values highlight substantial improvements in accuracy compared to individual streams, particularly for actions like KnockOver (15.3%) and TakePhoto (12.5%). However, certain actions, such as WieldKnife and HitWithObject, remain challenging, with relatively lower accuracies and frequent confusion with similar actions like ShootWithGun and Punch/Slap, respectively. The results underscore the effectiveness of multi-stream fusion in enhancing the accuracy and robustness of action recognition, especially in distinguishing between closely related human activities.

**Table 4** Comparison of different fusion feature model recognition performance on NTU RGB+D 120 with the Cross-View benchmark.

| Actions         | Joint+motion |                   | Temporal+motion |                              |                   | Joint+temporal+motion |                              |                   |
|-----------------|--------------|-------------------|-----------------|------------------------------|-------------------|-----------------------|------------------------------|-------------------|
|                 | Acc(%)       | Similar Action    | Acc(%)          | Acc $\uparrow\downarrow$ (%) | Similar Action    | Acc(%)                | Acc $\uparrow\downarrow$ (%) | Similar Action    |
| Punch/slap      | 49.1         | HitWithObject     | 54.1            | $\uparrow 5$                 | HitWithObject     | 60.3                  | $\uparrow 6.2$               | HitWithObject     |
| Kicking         | 70.1         | StepOnFoot        | 72.9            | $\uparrow 1.8$               | StepOnFoot        | 74.9                  | $\uparrow 2.0$               | StepOnFoot        |
| Pushing         | 67.9         | KnockOver         | 70.8            | $\uparrow 2.9$               | KnockOver         | 80.3                  | $\uparrow 9.4$               | KnockOver         |
| Pat on the back | 58.1         | Touch pocket      | 71.2            | $\uparrow 13.1$              | Touch pocket      | 84.1                  | $\uparrow 12.9$              | Touch pocket      |
| Point finger    | 59.9         | RockPaperScissors | 63.9            | $\uparrow 4.0$               | RockPaperScissors | 78.1                  | $\uparrow 14.2$              | RockPaperScissors |
| Hugging         | 86.9         | High-five         | 90.6            | $\uparrow 3.7$               | High-five         | 88.3                  | $\downarrow 2.3$             | High-five         |
| Giving object   | 51.6         | GrabStuff         | 49.8            | $\downarrow 1.8$             | GrabStuff         | 59.7                  | $\uparrow 9.9$               | GrabStuff         |
| Touch pocket    | 57.3         | Pat on the back   | 55.2            | $\downarrow 2.1$             | Pat on the back   | 57.3                  | $\uparrow 2.1$               | Pat on the back   |
| Shake hands     | 64.2         | Cheers            | 58.9            | $\downarrow 5.3$             | Cheers            | 73.4                  | $\uparrow 14.5$              | Cheers            |
| Walk towards    | 91.1         | Walk apart        | 89.9            | $\downarrow 1.2$             | Walk apart        | 91.4                  | $\uparrow 1.5$               | Walk apart        |
| Walk apart      | 86.8         | Walk towards      | 92.4            | $\uparrow 5.6$               | Walk towards      | 90.9                  | $\downarrow 1.5$             | Walk towards      |
| HitWithObject   | 30.5         | Punch/slap        | 45.4            | $\uparrow 14.9$              | Punch/slap        | 45.1                  | $\downarrow 0.3$             | Punch/slap        |
| WieldKnife      | 43.9         | ShootWithGun      | 35.2            | $\downarrow 8.7$             | ShootWithGun      | 43.3                  | $\uparrow 8.1$               | ShootWithGun      |
| KnockOver       | 65.1         | Pushing           | 66.0            | $\uparrow 0.9$               | Pushing           | 81.3                  | $\uparrow 15.3$              | Pushing           |
| GrabStuff       | 53.8         | CarryObject       | 64.0            | $\uparrow 10.2$              | CarryObject       | 72.4                  | $\uparrow 8.4$               | CarryObject       |
| ShootWithGun    | 43.5         | WieldKnife        | 46.9            | $\uparrow 3.4$               | WieldKnife        | 63.9                  | $\uparrow 17.0$              | WieldKnife        |
| StepOnFoot      | 65.2         | Kicking           | 73.9            | $\uparrow 8.7$               | Kicking           | 79.2                  | $\uparrow 5.3$               | Kicking           |
| High-five       | 71.9         | Hugging           | 79.7            | $\uparrow 7.8$               | Hugging           | 90.2                  | $\uparrow 10.5$              | Hugging           |
| CheersAndDri    | 63.8         | Shake             | 64.0            | $\uparrow 0.2$               | Shake             | 83.9                  | $\uparrow 19.9$              | Shake             |

| nk                |      | hands             |      |       | hands            |      |       | hands             |
|-------------------|------|-------------------|------|-------|------------------|------|-------|-------------------|
| CarryObject       | 84.3 | GrabStuff         | 89.6 | ↑5.3  | GrabStuff        | 89.6 | --    | GrabStuff         |
| TakePhoto         | 56.8 | ShootWith<br>hGun | 76.0 | ↑19.2 | ShootWith<br>Gun | 63.5 | ↓12.5 | ShootWith<br>hGun |
| Follow            | 55.9 | SupportSomebody   | 80.5 | ↑24.6 | SupportSomebody  | 81.1 | ↑0.6  | SupportSomebody   |
| Whisper           | 68.0 | SupportSomebody   | 74.1 | ↑6.1  | SupportSomebody  | 72.7 | ↓1.4  | SupportSomebody   |
| ExchangeThings    | 61.4 | Giving<br>object  | 76.8 | ↑15.4 | Giving<br>object | 74.0 | ↓2.8  | Giving<br>object  |
| SupportSomebody   | 66.7 | Whisper           | 83.3 | ↑16.6 | Whisper          | 83.4 | ↑0.1  | Whisper           |
| RockPaperScissors | 64.4 | Point<br>finger   | 81.3 | ↑16.9 | Point<br>finger  | 75.6 | ↓5.7  | Point<br>finger   |

**Acc:** The accuracy of the model in recognizing the action.

**Acc↑:** The improvement (if any) in accuracy when using joint-temporal-motion fusion compared to individual streams.

**Acc↓:** The descend (if any) in accuracy when using joint-temporal-motion fusion compared to individual streams.

**Similar Action:** The most frequent misclassified or confused action.

**Table 5** compares the performance of different fusion feature models for action recognition across three streams—joint-motion, temporal-motion, and joint-temporal-motion—on the NTU-RGB+D 120 dataset using the Cross-Subject benchmark. For joint motion, actions such as Hugging and HitWithObject exhibit relatively high accuracies (81.8% and 85.5%, respectively), while actions like WieldKnife and KnockOver have much lower accuracies (24.5% and 31.6%, respectively).

In the temporal-motion stream, WalkTowards achieves the highest accuracy (95.2%), followed closely by ShakeHands and Hugging (95.2% and 78.8%, respectively), with notable improvements in accuracy for most actions. The joint-temporal-motion fusion consistently provides enhanced recognition performance across most actions. For instance, WalkTowards achieves an accuracy of 98.4%, Hugging improves to 89.1%, and ShakeHands reaches 95.8%. Several actions, such as Pushing and StepOnFoot, also show substantial improvements in accuracy (up to 139.3% for Pushing). Acc(↑%) values indicate significant improvements in recognition accuracy when utilizing joint-temporal-motion fusion. For example, actions like Pushing, Kicking, and TouchPocket benefit from substantial performance boosts, suggesting that combining joint and temporal information greatly aids in disambiguating these actions. The similar action column highlights the challenges of the task, with certain actions frequently being confused with others. For example, Punch/slap is often misclassified as HitWithObject across all streams, while StepOnFoot is frequently confused with Kicking.

**Table 5** Comparison of different fusion feature model recognition performance on NTU RGB+D 120 with the Cross-Subject benchmark.

| Actions    | Joint+motion |                | Temporal+motion |          |                | Joint+temporal+motion |          |                |
|------------|--------------|----------------|-----------------|----------|----------------|-----------------------|----------|----------------|
|            | Acc(%)       | Similar Action | Acc(%)          | Acc↑↓(%) | Similar Action | Acc(%)                | Acc↑↓(%) | Similar Action |
| Punch/slap | 61.7         | HitWithObject  | 62.0            | ↑0.3     | HitWithObject  | 68.6                  | ↑6.6     | HitWithObject  |



|                   |      |                   |      |       |                   |      |       |                   |
|-------------------|------|-------------------|------|-------|-------------------|------|-------|-------------------|
| Kicking           | 68.5 | StepOnFoot        | 65.6 | ↓2.9  | StepOnFoot        | 79.0 | ↑13.4 | StepOnFoot        |
| Pushing           | 70.3 | KnockOver         | 72.1 | ↑1.8  | KnockOver         | 86.6 | ↑14.5 | KnockOver         |
| Pat on the back   | 65.9 | Touch pocket      | 60.5 | ↓5.4  | Touch pocket      | 81.5 | ↑21.0 | Touch pocket      |
| Point finger      | 65.9 | RockPaperScissors | 56.9 | ↓9.0  | RockPaperScissors | 76.4 | ↑19.5 | RockPaperScissors |
| Hugging           | 81.8 | High-five         | 86.9 | ↑5.1  | High-five         | 91.6 | ↑4.7  | High-five         |
| Giving object     | 40.9 | GrabStuff         | 46.7 | ↑5.8  | GrabStuff         | 62.7 | ↑16   | GrabStuff         |
| Touch pocket      | 65.1 | Pat on the back   | 68.9 | ↑3.8  | Pat on the back   | 82.5 | ↑13.6 | Pat on the back   |
| Shake hands       | 65.1 | Cheers            | 64.7 | ↓0.4  | Cheers            | 77.2 | ↑12.5 | Cheers            |
| Walk towards      | 63.4 | Walk apart        | 60.9 | ↓2.5  | Walk apart        | 90.5 | ↑29.6 | Walk apart        |
| Walk apart        | 87.9 | Walk towards      | 95.2 | ↑7.3  | Walk towards      | 88.4 | ↓6.8  | Walk towards      |
| HitWithObject     | 85.5 | Punch/slap        | 87.7 | ↑2.2  | Punch/slap        | 87.4 | ↓0.3  | Punch/slap        |
| WieldKnife        | 24.5 | ShootWithGun      | 36.9 | ↑12.4 | ShootWithGun      | 42.7 | ↑5.8  | ShootWithGun      |
| KnockOver         | 31.6 | Pushing           | 36.6 | ↑5.0  | Pushing           | 75.9 | ↑39.3 | Pushing           |
| GrabStuff         | 64.2 | CarryObject       | 66.1 | ↑1.9  | CarryObject       | 73.2 | ↑7.1  | CarryObject       |
| ShootWithGun      | 46.3 | WieldKnife        | 59.3 | ↑13.0 | WieldKnife        | 54.4 | ↓4.9  | WieldKnife        |
| StepOnFoot        | 49.9 | Kicking           | 48.5 | ↓1.4  | Kicking           | 85.2 | ↑36.7 | Kicking           |
| High-five         | 76.5 | Hugging           | 78.8 | ↑2.3  | Hugging           | 89.1 | ↑10.3 | Hugging           |
| CheersAndDrink    | 78.1 | Shake hands       | 95.2 | ↑17.1 | Shake hands       | 95.8 | ↑0.6  | Shake hands       |
| CarryObject       | 82.5 | GrabStuff         | 84.2 | ↑1.7  | GrabStuff         | 91.7 | ↑7.5  | GrabStuff         |
| TakePhoto         | 62.2 | ShootWithGun      | 73.2 | ↑11.0 | ShootWithGun      | 75.7 | ↑2.5  | ShootWithGun      |
| Follow            | 68.4 | SupportSomebody   | 88.9 | ↑20.5 | SupportSomebody   | 85.4 | ↓3.5  | SupportSomebody   |
| Whisper           | 72.5 | SupportSomebody   | 78.5 | ↑6.0  | SupportSomebody   | 78.8 | ↑0.3  | SupportSomebody   |
| ExchangeThings    | 67.1 | Giving object     | 75.5 | ↑8.4  | Giving object     | 74.3 | ↓1.2  | Giving object     |
| SupportSomebody   | 66.9 | Whisper           | 79.0 | ↑12.1 | Whisper           | 82.4 | ↑3.4  | Whisper           |
| RockPaperScissors | 66.0 | Point finger      | 77.3 | ↑11.3 | Point finger      | 83.0 | ↑5.7  | Point finger      |

**Acc:** The accuracy of the model in recognizing the action.

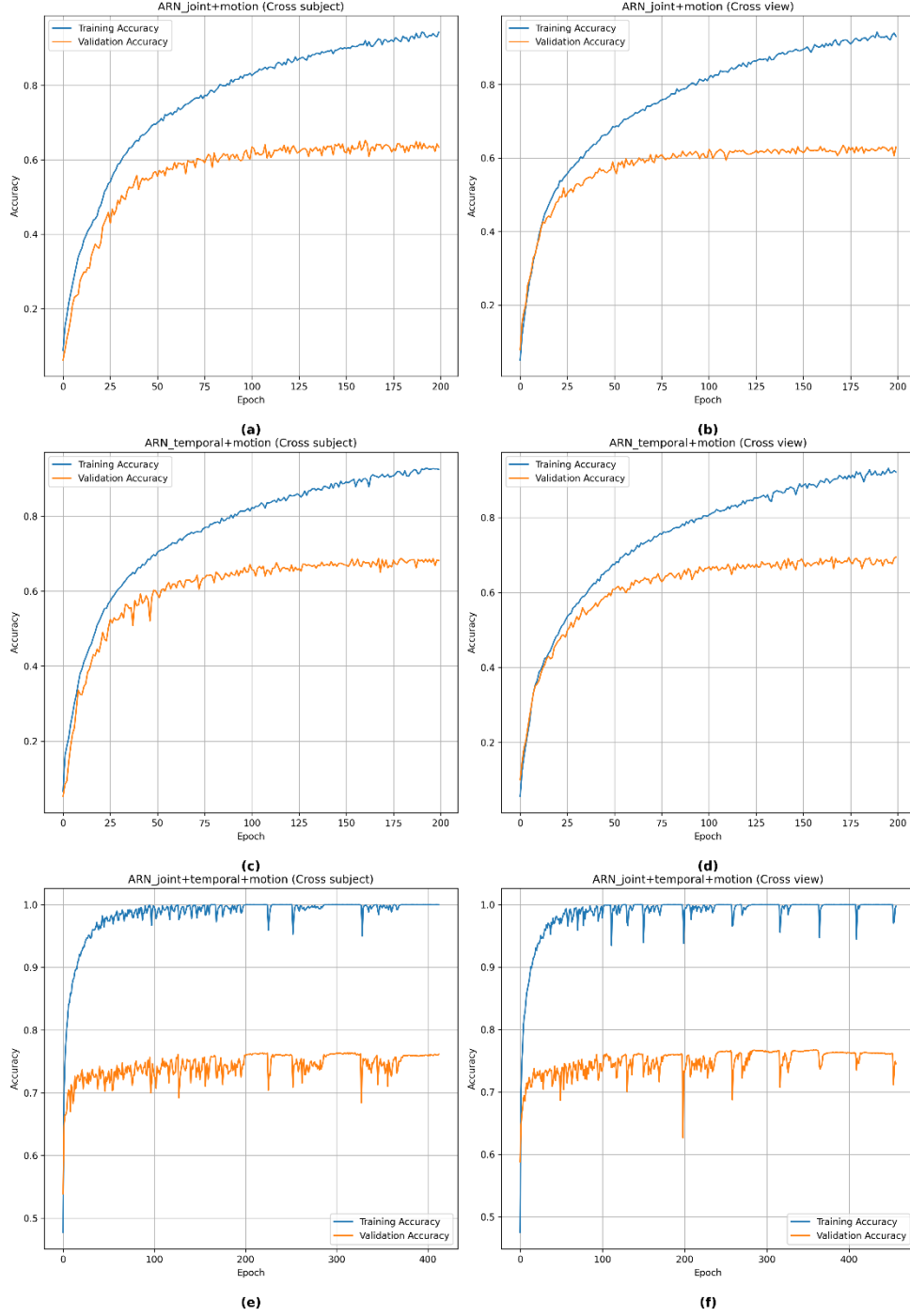
**Acc $\uparrow$ :** The improvement (if any) in accuracy when using joint-temporal-motion fusion compared to individual streams.

**Acc $\downarrow$ :** The descent (if any) in accuracy when using joint-temporal-motion fusion compared to individual streams.

**Similar Action:** The most frequent misclassified or confused action.

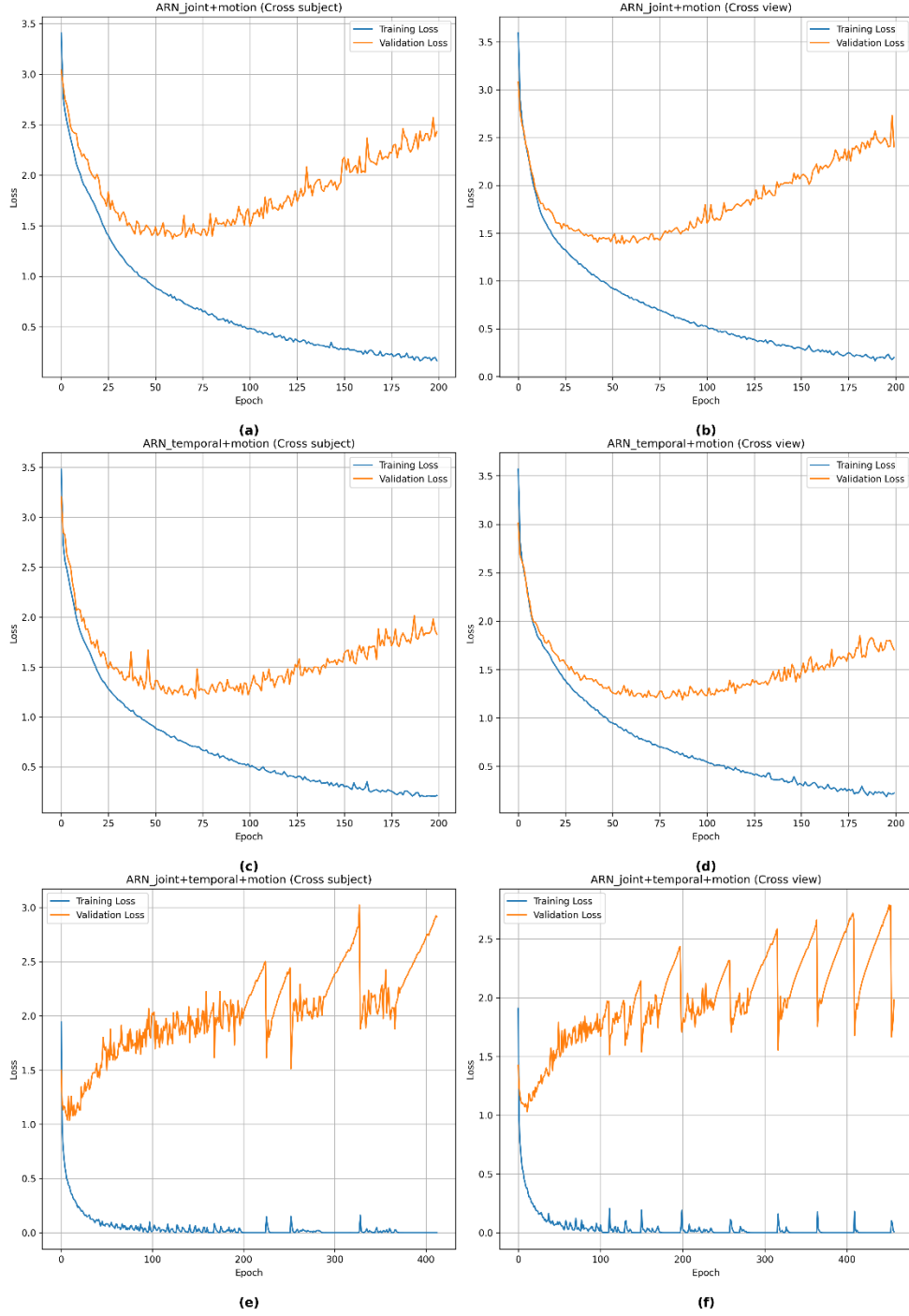
In summary, our proposed ARN-LSTM approach with the joint-temporal-motion fusion consistently outperforms both individual streams (joint-motion and temporal-motion), achieving superior accuracy and minimizing confusion between similar actions. The results indicate that integrating multiple information streams is crucial for improving recognition accuracy, particularly for complex and similar

human actions.



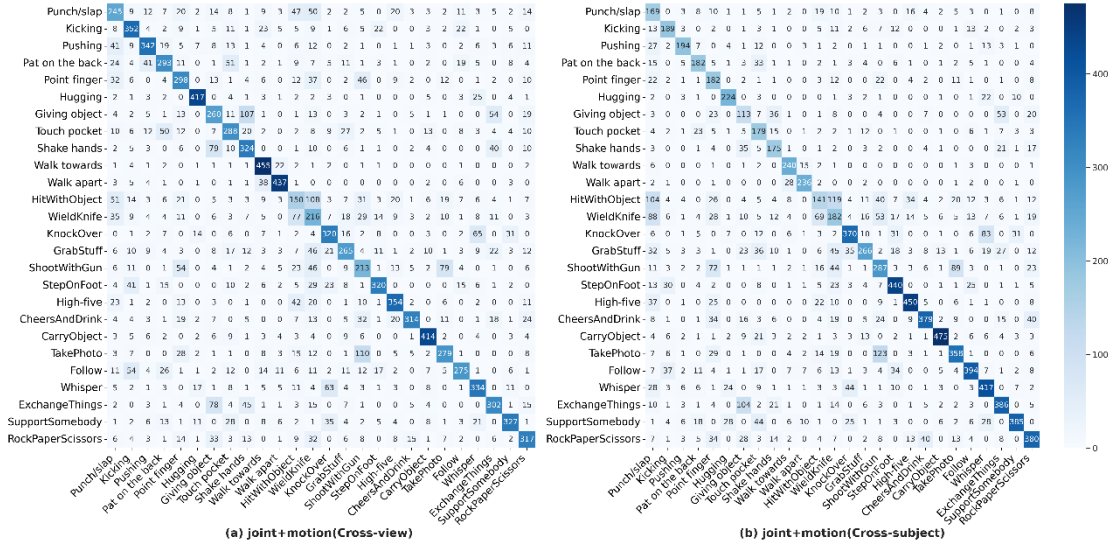
**Figure 7 Accuracy curves on the NTU RGB+D 120 dataset**

Figure 7 the training accuracy improves steadily across all models, reaching high values, while the validation accuracy plateaus significantly earlier, indicating a gap between training and validation performance. Particularly, the joint-temporal-motion models (e, f) show the largest training-validation discrepancy, suggesting potential overfitting as the training accuracy approaches near-perfect levels, while the validation accuracy remains relatively lower and stable.



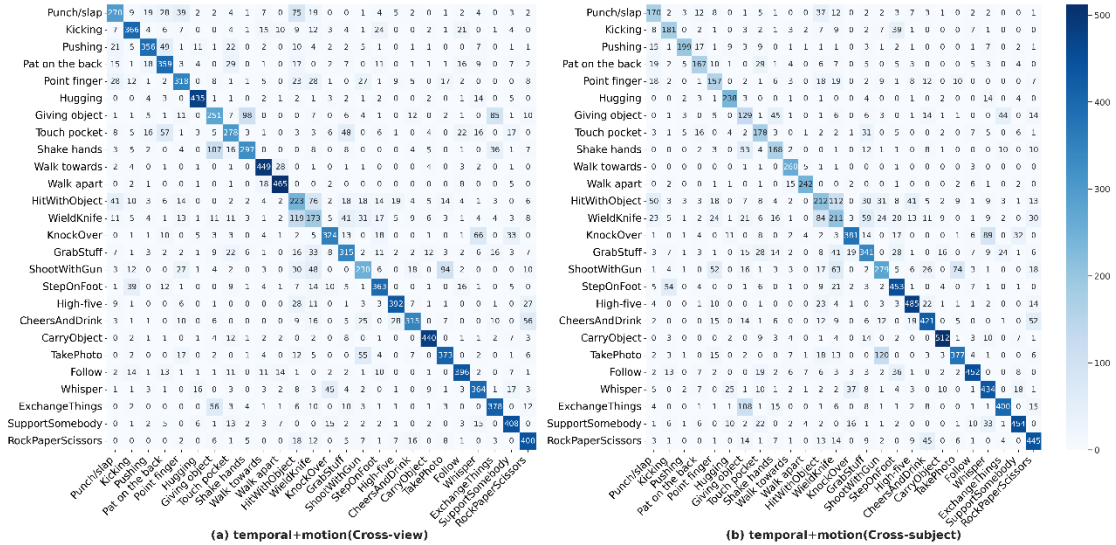
**Figure 8 Loss curves on the NTU RGB+D 120 dataset**

Figure 8 the training loss decreases steadily for all models, indicating effective learning, while the validation loss stabilizes or increases after a certain point, suggesting potential overfitting. The joint-temporal-motion models (e, f) exhibit the most pronounced overfitting, as the validation loss increases sharply compared to other models.



**Figure 9 Confusion matrix of ARN-LSTM with joint motion on the NTU RGB+D 120 dataset.**

Figure 9 confusion matrix compares joint-motion-based models' performance across two benchmarks: (a) cross-view and (b) cross-subject action recognition. Both matrices show high accuracy along the diagonal, indicating strong model performance for most actions, though some actions exhibit confusion, particularly for the cross-subject case, where inter-subject variability introduces additional challenges.



**Figure 10 Confusion matrix of ARN-LSTM with temporal motion on the NTU RGB+D 120 dataset.**

Figure 10 the confusion matrices illustrate the performance of the ARN-LSTM method using temporal and motion features on the NTU RGB+D 120 dataset with the cross-view and cross-subject benchmark. The diagonal dominance in both matrices indicates that the model correctly classifies most of the 30 action classes, such as "Kicking," "Wield Knife," and "Support Somebody," with high accuracy. However, there are notable misclassifications, particularly between similar actions like "Hit with Object" and "Punch/Slap," or "Walk towards" and "Walk apart," which appear frequently confused across both settings. Despite these errors, the overall performance remains strong, as most actions have high counts on the diagonal, indicating correct classifications. The system performs consistently well in both experimental conditions, though there is some variation in accuracy across specific action classes,

reflecting the challenges of distinguishing actions with overlapping motion characteristics.

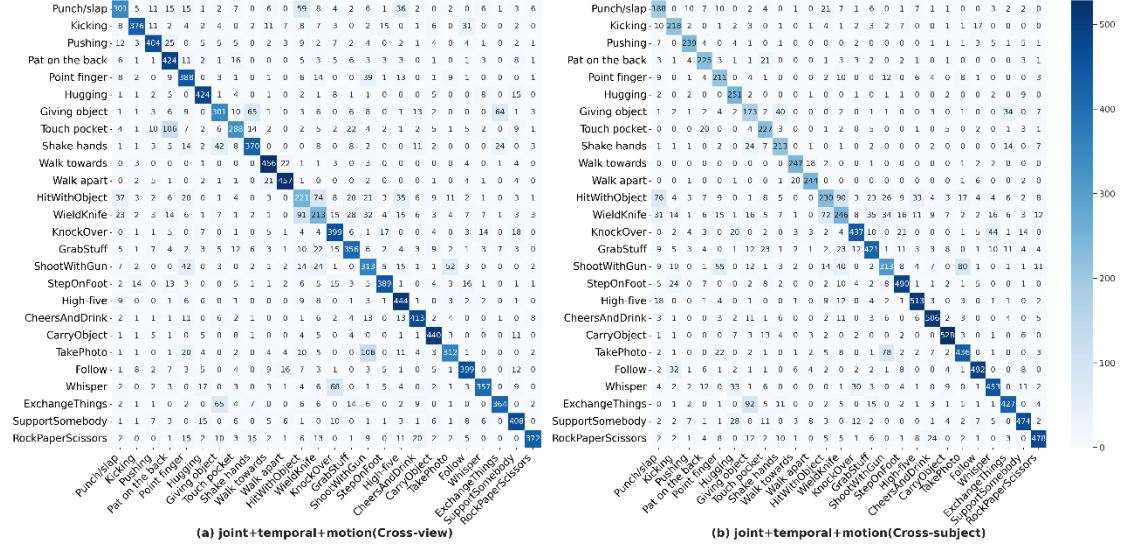


**Figure 11 Confusion matrix of ARN-LSTM with joint, temporal and motion features on the NTU RGB+D 120 dataset.**

Figure 11 the confusion matrices illustrates the performance of the ARN-LSTM method using joint, temporal and motion features on the NTU RGB+D 120 dataset with the cross-view and cross-subject. The diagonal dominance in both matrices indicates a high accuracy across most of the 30 action classes, such as "Kicking," "Pushing," and "Support somebody," where the model consistently makes correct predictions. However, there are notable misclassifications, particularly between actions with similar motion dynamics, such as "Punch/slap" and "Hit with object," which are frequently confused in both settings. These results suggest that while the system effectively distinguishes many actions, it faces challenges in separating actions with overlapping visual or motion characteristics, especially when there are variations in viewpoint or subject. Despite these challenges, the overall performance remains strong, as evidenced by the large number of correct classifications in both cross-view and cross-subject experiments.

## 6. Conclusion

In this paper, we introduced ARN-LSTM, a novel multi-stream model for action recognition that effectively combines joint, motion, and temporal features. The model can capture complex spatial-temporal dependencies by integrating Attention Relation Networks and a TD-LSTM. The proposed ARN-LSTM approach is a sophisticated neural network model adept at processing diverse forms of object data, including federated streams, joint streams, temporal streams, and general relational data. It leverages relational modeling and attention mechanisms to enhance model performance. The flexible parameter configuration facilitates the implementation of various network architectures. On the two large-scale datasets, NTU RGB+D 60 and NTU RGB+D 120 dataset, the proposed ARN-LSTM leads to effective performance on group activity recognition tasks. Future work will focus on extending the model to handle larger datasets and exploring its application to real-time action recognition systems. Inspired by [9, 48, 49], we will also attempt to use higher-level information to improve the results, such as the Graph Convolutional Neural Network method.

## Acknowledgments

This work was partly supported by the University Characteristic Innovation Projects of Guangdong Province of China (Grant: 2023KTSCX196). The authors would like to thank the anonymous referees for their insightful comments, which greatly improved the quality of this paper.

### **Author contributions**

Chuanchuan Wang wrote the main manuscript text and constructed the main idea of the proposed framework. Ahmad Sufril Azlan Mohamed reviewed the manuscript and gave suggestions for writing and publishing. Xiang Li prepared the first results of the framework and helped develop the proposed framework. Xiao Yang helped to preprocess the results of the experiment. All of the authors edited the submitted version of the manuscript.

### **Competing interests**

The authors declare that they have no known conflict of competing interests, this work is only for study.

### **Data Availability**

The datasets used for the study can be available at <https://doi.org/10.6084/m9.figshare.27427188.v1>.

### **References**

- [1] JAMIL F, AHMAD S, WHANGBO T K, et al. Improving blockchain performance in clinical trials using intelligent optimal transaction traffic control mechanism in smart healthcare applications [J]. Computers & Industrial Engineering, 2022, 170(108327).
- [2] NIKPOUR B, SINODINOS D, ARMANFARD N. Deep Reinforcement Learning in Human Activity Recognition: A Survey and Outlook [J]. IEEE Transactions on Neural Networks and Learning Systems, 2024,
- [3] SONG L, HE Y, YUAN H, et al. Human Action Recognition Based on Spatial Temporal Adaptive Residual Graph Convolutional Networks with Attention Mechanism; proceedings of the 2024 43rd Chinese Control Conference (CCC), F, 2024 [C]. IEEE.
- [4] HUANG J, ZHENG R, CHENG Y, et al. Interactive semantics neural networks for skeleton-based human interaction recognition [J]. The Visual Computer, 2024, 1-14.
- [5] GAO Z, LIU X, WANG A K, et al. A simulated two-stream network via multilevel distillation of reviewed features and decoupled logits for video action recognition [J]. The Visual Computer, 2024,
- [6] SHENG B, LI P, ALI R, et al. Improving video temporal consistency via broad learning system [J]. IEEE Transactions on Cybernetics, 2021, 52(7): 6662-75.
- [7] ASKARI F, RAMAPRASAD R, CLARK J J, et al. Interaction Classification with Key Actor Detection in Multi-Person Sports Videos; proceedings of the Proceedings of the IEEE/CVF Conference on Computer Vision and Pattern Recognition, F, 2022 [C].
- [8] YAN S, XIONG Y, LIN D. Spatial temporal graph convolutional networks for skeleton-based action recognition; proceedings of the Proceedings of the AAAI conference on artificial intelligence, F, 2018 [C].
- [9] WANG H, WANG Y, YAN S, et al. Merge-and-Split Graph Convolutional Network for Skeleton-Based Interaction Recognition [J]. Cyborg and Bionic Systems, 2024, 5(0102).
- [10] LIU J, WANG G, DUAN L-Y, et al. Skeleton-Based Human Action Recognition With Global Context-Aware Attention LSTM Networks [J]. Ieee Transactions on Image Processing, 2018, 27(4):

1586-99.

- [11] XIE Z, ZHANG W, SHENG B, et al. BaGFN: broad attentive graph fusion network for high-order feature interactions [J]. IEEE Transactions on Neural Networks and Learning Systems, 2021, 34(8): 4499-513.
- [12] ZHOU Y, CHEN Z, LI P, et al. FSAD-Net: feedback spatial attention dehazing network [J]. IEEE transactions on neural networks and learning systems, 2022, 34(10): 7719-33.
- [13] LIN X, SUN S, HUANG W, et al. EAPT: efficient attention pyramid transformer for image processing [J]. IEEE Trans Multimedia, 2021, 25(50-61).
- [14] AOUIDJIA K, SHENG B, LI P, et al. Efficient body motion quantification and similarity evaluation using 3-D joints skeleton coordinates [J]. IEEE Transactions on Systems, Man, and Cybernetics: Systems, 2019, 51(5): 2774-88.
- [15] WANG C, MOHAMED A S A. Attention Relational Network for Skeleton-Based Group Activity Recognition [J]. IEEE Access, 2023, 11(129230-9).
- [16] CHEN X, GUO H, WANG G, et al. Motion feature augmented recurrent neural network for skeleton-based dynamic hand gesture recognition; proceedings of the 2017 IEEE International Conference on Image Processing (ICIP), F, 2017 [C]. IEEE.
- [17] GUAN Y, PLÖTZ T. Ensembles of deep lstm learners for activity recognition using wearables [J]. Proceedings of the ACM on interactive, mobile, wearable and ubiquitous technologies, 2017, 1(2): 1-28.
- [18] TRAN D, BOURDEV L, FERGUS R, et al. Learning spatiotemporal features with 3d convolutional networks; proceedings of the Proceedings of the IEEE international conference on computer vision, F, 2015 [C].
- [19] DU Y, WANG W, WANG L. Hierarchical recurrent neural network for skeleton based action recognition; proceedings of the Proceedings of the IEEE conference on computer vision and pattern recognition, F, 2015 [C].
- [20] LIU J, SHAHROUDY A, XU D, et al. Spatio-temporal lstm with trust gates for 3d human action recognition; proceedings of the Computer Vision—ECCV 2016: 14th European Conference, Amsterdam, The Netherlands, October 11-14, 2016, Proceedings, Part III 14, F, 2016 [C]. Springer.
- [21] URABE S, INOUE K, YOSHIOKA M. Cooking activities recognition in egocentric videos using combining 2DCNN and 3DCNN; proceedings of the Proceedings of the Joint Workshop on Multimedia for Cooking and Eating Activities and Multimedia Assisted Dietary Management, F, 2018 [C].
- [22] ULLAH H, MUNIR A. Human action representation learning using an attention-driven residual 3dcnn network [J]. Algorithms, 2023, 16(8): 369.
- [23] HOU Y, LI Z, WANG P, et al. Skeleton optical spectra-based action recognition using convolutional neural networks [J]. IEEE Trans Circuits Syst Video Technol, 2016, 28(3): 807-11.
- [24] CHEN Z, LI S, YANG B, et al. Multi-scale spatial temporal graph convolutional network for skeleton-based action recognition; proceedings of the Proceedings of the AAAI conference on artificial intelligence, F, 2021 [C].
- [25] NIKPOUR B, ARMANFARD N. Spatio-temporal hard attention learning for skeleton-based activity recognition [J]. Pattern Recognit, 2023, 139(109428).
- [26] WU C, WU X-J, XU T, et al. Motion complement and temporal multifocusing for skeleton-based action recognition [J]. IEEE Trans Circuits Syst Video Technol, 2023, 34(1): 34-45.
- [27] JANG S, LEE H, KIM W J, et al. Multi-scale Structural Graph Convolutional Network for Skeleton-based Action Recognition [J]. IEEE Trans Circuits Syst Video Technol, 2024,
- [28] ZHAO Z, CHEN Z, LI J, et al. Glimpse and zoom: Spatio-temporal focused dynamic network for



- skeleton-based action recognition [J]. IEEE Trans Circuits Syst Video Technol, 2024,
- [29] LI C, MAO Y, HUANG Q, et al. Scale-Aware Graph Convolutional Network with Part-Level Refinement for Skeleton-Based Human Action Recognition [J]. IEEE Trans Circuits Syst Video Technol, 2023,
- [30] LIU D, HUANG Y, LIU Z, et al. A skeleton-based assembly action recognition method with feature fusion for human-robot collaborative assembly [J]. Journal of Manufacturing Systems, 2024, 76(553-66.
- [31] WANG S, KONG J, JIANG M, et al. Multiple depth-levels features fusion enhanced network for action recognition [J]. J Vis Commun Image Represent, 2020, 73(102929.
- [32] SONG C, LIN Y, GUO S, et al. Spatial-temporal synchronous graph convolutional networks: A new framework for spatial-temporal network data forecasting; proceedings of the Proceedings of the AAAI conference on artificial intelligence, F, 2020 [C].
- [33] SHI L, ZHANG Y, CHENG J, et al. Skeleton-based action recognition with directed graph neural networks; proceedings of the Proceedings of the IEEE/CVF conference on computer vision and pattern recognition, F, 2019 [C].
- [34] SHI L, ZHANG Y, CHENG J, et al. Two-stream adaptive graph convolutional networks for skeleton-based action recognition; proceedings of the Proceedings of the IEEE/CVF conference on computer vision and pattern recognition, F, 2019 [C].
- [35] SANTORO A, RAPOSO D, BARRETT D G, et al. A simple neural network module for relational reasoning [J]. Advances in neural information processing systems, 2017, 30(
- [36] PEREZ M, LIU J, KOT A C. Interaction relational network for mutual action recognition [J]. IEEE Trans Multimedia, 2021, 24(366-76.
- [37] BISHOP C M, NASRABADI N M. Pattern recognition and machine learning [M]. Springer, 2006.
- [38] EDITION F, PAPOULIS A, PILLAI S U. Probability, random variables, and stochastic processes [M]. McGraw-Hill Europe: New York, NY, USA, 2002.
- [39] SHAHROUDY A, LIU J, NG T-T, et al. Ntu rgb+ d: A large scale dataset for 3d human activity analysis; proceedings of the Proceedings of the IEEE conference on computer vision and pattern recognition, F, 2016 [C].
- [40] LIU J, SHAHROUDY A, PEREZ M, et al. NTU RGB+D 120: A Large-Scale Benchmark for 3D Human Activity Understanding [J]. IEEE Trans Pattern Anal Mach Intell, 2020, 42(10): 2684-701.
- [41] FAWCETT T. An introduction to ROC analysis [J]. Pattern Recognit Lett, 2006, 27(8): 861-74.
- [42] LIU J, SHAHROUDY A, XU D, et al. Spatio-Temporal LSTM with Trust Gates for 3D Human Action Recognition; proceedings of the 14th European Conference on Computer Vision (ECCV), Amsterdam, NETHERLANDS, F 2016 Oct 08-16, 2016 [C]. 2016.
- [43] SONG S, LAN C, XING J, et al. An end-to-end spatio-temporal attention model for human action recognition from skeleton data; proceedings of the Proceedings of the AAAI conference on artificial intelligence, F, 2017 [C].
- [44] CHENG K, ZHANG Y, HE X, et al. Skeleton-based action recognition with shift graph convolutional network; proceedings of the Proceedings of the IEEE/CVF conference on computer vision and pattern recognition, F, 2020 [C].
- [45] SU Y, LIN G, WU Q. Self-supervised 3d skeleton action representation learning with motion consistency and continuity; proceedings of the Proceedings of the IEEE/CVF international conference on computer vision, F, 2021 [C].
- [46] SONG Y-F, ZHANG Z, SHAN C, et al. Constructing stronger and faster baselines for skeleton-

- based action recognition [J]. IEEE Trans Pattern Anal Mach Intell, 2022, 45(2): 1474-88.
- [47] YANG P, WANG Q, CHEN H, et al. Position-aware spatio-temporal graph convolutional networks for skeleton-based action recognition [J]. IET Computer Vision, 2023, 17(7): 844-54.
- [48] LI S, HE X, SONG W, et al. Graph Diffusion Convolutional Network for Skeleton Based Semantic Recognition of Two-Person Actions [J]. IEEE Trans Pattern Anal Mach Intell, 2023,
- [49] YANG Y, CHEN H, LIU Z, et al. Action recognition with multi-stream motion modeling and mutual information maximization [J]. arXiv preprint arXiv:230607576, 2023,